Visualization of spatially and temporally regulated N-WASP activity during cytoskeletal reorganization in living cells

Michael E. Ward*, Jane Y. Wu†‡, and Yi Rao*‡

*Department of Anatomy and Neurobiology, Washington University School of Medicine, 660 South Euclid Avenue, Box 8108, St. Louis, MO 63110; and †Departments of Pediatrics, Cell and Developmental Biology, and Pharmacology, John F. Kennedy Center for Research on Human Development, MRBIII Room 7110, Vanderbilt University Medical Center, 465 21st Avenue South, Nashville, TN 37232-8548

Edited by Lily Y. Jan, University of California School of Medicine, San Francisco, CA, and approved November 20, 2003 (received for review September 29, 2003)

Members of the WASP/WAVE family of proteins are key regulators of cytoskeletal reorganization across a diverse range of cellular processes. Despite a wealth of biochemical data about WASP/WAVE regulation *in vitro*, our understanding of the *in vivo* regulation of these proteins is hampered by the inability to monitor subcellular regulation of their activities in living cells. Here we establish a fluorescence resonance energy transfer-based approach to visualize spatial and temporal regulation of neuronal Wiskott–Aldrich syndrome protein (N-WASP) activity in living cells. Using time-lapse microscopy, we characterize the activation of N-WASP in response to growth-factor stimulation, and we reveal that N-WASP is activated inside extending filopodia. Furthermore, we suggest a role of N-WASP in regulating membrane ruffling downstream of phosphatidylinositol 4,5-bisphosphate and Cdc42.

Cell migration is an important biological process during development, as well as a defining feature of tumor metastasis in pathogenesis. It is well established that regulation of the actin cytoskeleton is crucial for normal cell migration. Several mechanisms are known to regulate actin dynamics, ranging from the control of actin polymerization to the regulation of actin filament branching and filament severing.

Neuronal Wiskott–Aldrich syndrome protein (N-WASP) is a member of the WASP/WAVE protein family and an important cytoskeletal regulator in a number of cellular processes, including cell migration, neurite extension, vesicle trafficking, growth-factor signaling, and actin-based motility of intracellular pathogens (1–5). WASP/WAVE proteins promote formation of actin branches at 70° angle to preformed actin filaments (6). N-WASP is activated by other intracellular molecules, including phosphatidylinositol 4,5-bisphosphate (PIP_2) and Cdc42, which are themselves regulated by extracellular signals. By integrating upstream signaling events, N-WASP acts as a molecular switch to activate the Arp2/3 complex in a spatially and temporally appropriate manner. It is well established that in its resting state, N-WASP exists in an autoinhibited conformation, wherein the verprolin–cofilin–acidic (VCA) domain in the C terminus of N-WASP is masked by an intramolecular interaction with the N-terminal GTPase-binding domain (GBD) (7–11). Structural and biochemical studies have shown that upon coordinated binding of PIP_2 and Cdc42-GTP to the basic domain and GBD of N-WASP, respectively, a dramatic conformational change ensues, resulting in the release of the C-terminal part of N-WASP and activation of the bound Arp2/3 complex (9–11) (see Fig. 1*a*).

Although such biochemical studies have revealed much about the regulation of N-WASP *in vitro*, little is known about how N-WASP is regulated *in vivo*. We have now been able to establish a method to monitor N-WASP activity in living cells by using a fluorescence resonance energy transfer (FRET)-based reporter protein. We show that this reporter displays changes in FRET efficiency after exposure to known regulators of N-WASP activity. Using this reporter in time-lapse microscopy, we then characterize the activation of N-WASP in living cells in response to growth-factor stimulation, and we reveal that N-WASP is activated at the peaks of membrane ruffles. Furthermore, we show that N-WASP is activated in extending filopodia after growth factor stimulation.

Materials and Methods

Plasmids. Stinger was created by first substituting citrine lacking 11 C-terminal amino acids (kindly provided by Roger Tsien, University of California at San Diego, La Jolla) for enhanced yellow fluorescent protein (YFP) in pRaichu-Ras (kindly provided by Michiyuki Matsuda, Osaka University, Osaka). Then, rat N-WASP lacking 30 N-terminal amino acids was substituted for Ras in this citrine-pRaichu-Ras construct.

Cells. HEK-293 cells and COS-7 cells were grown in DMEM (high glucose) containing 10% FCS. For epidermal growth factor (EGF) stimulation experiments, cells were serum-starved overnight in L-15 plus 0.1% FCS before EGF exposure. For cell imaging, cells were cultured in L-15 (phenol-red free, with 10% FCS for all experiments except those involving EGF stimulation).

***In Vitro* Spectrofluorimetry.** HEK-293 cells were transfected by using calcium phosphate DNA precipitation. Cells were transfected with Stinger alone, Cdc42-N17 (an inactive Cdc42 mutant, hereafter referred to as Cdc42-DN) alone, or Cdc42-L61 (a constitutively active Cdc42 mutant, hereafter referred to as Cdc42-CA) alone. Forty-eight hours later, cells were lysed in 1 ml of ice-cold lysis buffer (20 mM Tris·HCl, pH 7.5/100 mM NaCl/4 mM $MgCl_2$/0.5% Triton X-100) with protease inhibitors (Complete, Roche). After lysis, cells were centrifuged at $50{,}000 \times g$ for 15 min at 4°C, and the supernatant was transferred to another tube. The preparation of synthetic PIP_2 liposomes used for *in vitro* spectroscopy experiments has been described previously (12). Because Cdc42-L61 expressed in bacteria was found to have relatively small effects on Stinger FRET, Cdc42-L61 expressed in HEK-293 cells was used in all *in vitro* assays. Before fluorescence spectra were taken, equal volumes of lysate from each of the following transfected samples were mixed together: Stinger lysate plus untransfected HEK-293 lysate (control), Stinger lysate plus Cdc42-L61 lysate, Stinger lysate plus Cdc42-N17, Stinger lysate plus untransfected HEK-293 lysate

This paper was submitted directly (Track II) to the PNAS office.

Abbreviations: N-WASP, neuronal Wiskott–Aldrich syndrome protein; PIP_2, phosphatidylinositol 4,5-bisphosphate; VCA, verprolin–cofilin–acidic; GBD, GTPase-binding domain; FRET, fluorescence resonance energy transfer; YFP, yellow fluorescent protein; CFP, cyan fluorescent protein; EGF, epidermal growth factor.

‡To whom correspondence may be addressed. E-mail: jane.wu@vanderbilt.edu or raoyi@pcg.wustl.edu.

www.pnas.org/cgi/doi/10.1073/pnas.0306258101

plus 10 μM PIP_2, Stinger lysate plus Cdc42-L61 lysate plus 10 μM PIP_2. To determine the minimum saturation of HEK-293-expressed Cdc42-L61, increasing amounts of untransfected HEK-293 cell lysate were added to Cdc42-L61 lysate. These combinations were then added to equal amounts of Stinger lysate as described above, and spectra were obtained with a fluorescent spectrometer (Perkin–Elmer MPF-44A) using an excitation wavelength of 433 nm. The minimum amount of Cdc42-L61 lysate needed to cause a maximal decrease in FRET efficiency was determined to be the saturating level of Cdc42. In experiments where subsaturating amounts of Cdc42 were used, 1 part of the minimal saturating Cdc42 lysate was mixed with 4 parts untransfected HEK-293 lysate, and then mixed with equal amounts of Stinger lysate as described above. In all cases, fluorescence spectra were taken 10 min after mixing the lysates together. To confirm the presence of intramolecular FRET, cell lysates were incubated with 50 μg/ml proteinase K at 37°C for 10 min and analyzed with the spectrofluorimeter.

Dual-Emission Ratio Imaging. HEK-293 or COS-7 cells were transfected as described above, and imaged either 24 or 48 h after transfection by using an upright BX61WI microscope (Olympus), a xenon illumination source (Lambda LS, Sutter Instruments, San Rafael, CA), and a water-immersion lens (0.9 numerical aperture). Cells were grown on poly-L-lysine-coated coverslips and transferred to a heated chamber (Delta T from Biopteches, Butler, PA) for imaging containing L-15 medium (plus 10% FCS for membrane ruffling experiments, plus 0.1% FCS for EGF stimulation and EGF-induced filopodia formation). Images were taken at the times indicated in the figures by using a cooled charge-coupled device camera (Coolsnap HQ, Roper Scientific) at 2×2 binning. For growth factor stimulation and Cdc42 overexpression imaging experiments, sequential CFP and CFP–YFP emission imaging was conduced with an ultrafast filter wheel (Lambda 10-2, Sutter). Filter combinations (Chroma Technology, Brattleboro, VT) were as follows: dichroic: 86008bs, (excitation:emission): CFP:CFP (S430/25, S465/30), CFP:YFP (S430/25, S550/50), and YFP:YFP for photobleaching experiments (S510/20, S465/30). To eliminate the possibility of motion-related artifacts during dual-emission ratio time-lapse imaging of subcellular structures, simultaneous CFP and CFP–YFP imaging was conducted by placing a Dual-View Micro-Imager (Optical Insights, Santa Fe, NM) between the microscope and camera. Excitation was conducted by using a 436/20 exciter and a OI-04-EM emission filter set (Chroma Technology). Exposure times varied depending on the expression level of Stinger, but were between 500 and 1,000 ms for membrane ruffling imaging, and between 1 and 5 s for filopodia imaging. After time-lapse imaging was complete, background-subtracted images were used to generate CFP/CFP–YFP images by using the ratio feature of Metamorph (Universal Imaging, Media, PA). For quantification of the effect of EGF on Stinger activity, regions were made around single cells by using background-subtracted images. The same regions were then used to quantify mean CFP and YFP intensities for each cell over time. For quantification of membrane ruffle and filopodia Stinger activity, regions were drawn around single membrane ruffles or filopodia, as well as the cytoplasm immediately adjacent to these structures. The same regions were then used to quantify mean CFP and YFP intensities for each structure and its adjacent cytoplasm.

Online Supporting Information. Time-lapse images are compiled into QuickTime movies (Movies 1–5, which are published as supporting information on the PNAS web site).

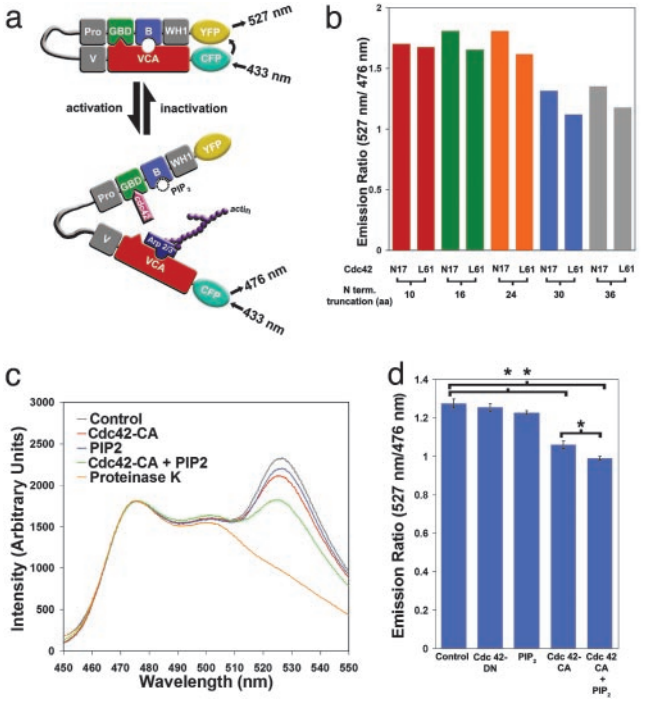

Fig. 1. Creation of a FRET-based reporter to measure the activation state of N-WASP. (*a*) Diagram of the N-WASP FRET protein. In its inactivated state, N-WASP is autoinhibited because of interactions between the C-terminal VCA domain and the N-terminal GBD and basic domain (B). Such autoinhibition juxtaposes the N-terminal YFP and C-terminal CFP, leading to high levels of FRET (emission at 527 nm when excited at 433 nm). Upon binding of Cdc42 and/or PIP_2, N-WASP becomes activated and interacts with the Arp2/3 complex, resulting in the formation of branched actin polymers. Simultaneously, the distance between the N-terminal YFP and C-terminal CFP increases, which in turn leads to low levels of FRET (emission at 476 nm when excited at 433 nm). (*b*) N-terminal truncation of the N-WASP FRET probe is necessary for activity-dependent FRET change. Because full-length N-WASP displayed little change in FRET after activation by Cdc42-CA, sequential deletions of the WH1 domain were made. These proteins were expressed in HEK-293 cells, and the level of FRET in the presence of inactive Cdc42 (Cdc42-N17) or constitutively active Cdc42 (Cdc42-L61) (represented by the ratio of emission at 527 nm to that at 476 nm) was measured with a spectrofluorimeter. (*c*) Cdc42 and PIP_2 result in synergistic changes in FRET efficiency of Stinger. FRET measurements were conducted on HEK-293 cell lysates containing Stinger only (control), Stinger plus Cdc42-CA, Stinger plus PIP_2, and Stinger plus Cdc42-CA plus PIP_2. Emission readings at 1-nm intervals were made in a spectrofluorimeter during excitation at 433 nm. FRET efficiency was determined by the ratio of YFP emission (527 nm) over CFP emission (476 nm). The sample containing Stinger only (control) was then treated with proteinase K to verify the existence of intramolecular FRET. All samples have been normalized to emission at 476 nm. Increases in the YFP emission signify increases in FRET efficiency, whereas decreases in YFP emission signify decreases in FRET efficiency. (*d*) Quantitation of Cdc42- and PIP_2-induced changes in Stinger FRET. Samples were prepared and analyzed as described for *c*, with the exception that saturating amounts of Cdc42-CA were used. Each bar represents the mean YFP/CFP (527/476) emission ratio of three independent samples. The error bars indicate SEM. *, Statistically significant differences between means ($P < 0.05$, two-sampled *t* test).

Results and Discussion

To monitor changes in N-WASP activity, we fused YFP to the N terminus, and CFP to the C terminus, of N-WASP to create a FRET-based reporter protein (Fig. 1*a*). Because the intramolecular distance between the C-terminal VCA domain and the N-terminal GBD of N-WASP is known to increase upon N-WASP activation (9), we hypothesized that our reporter would display decreased FRET efficiency during N-WASP activation. We began our studies with a fusion protein that was based on

full-length N-WASP, but found that addition of a constitutively active Cdc42 mutant did not result in any detectable change in its FRET efficiency. It is possible that the observed lack of regulated FRET efficiency was caused by too much flexibility between the N terminus of N-WASP and YFP. To overcome this problem, we used a shortened YFP lacking 11 C-terminal amino acid residues, and a number of N-WASP variants with 10 to 36 residues removed from the N terminus preceding the WASP homology 1 (WH1) domain. It has been shown that the first 34 N-terminal residues are not necessary for any known function of N-WASP (1, 11, 13). We then tested these fusion proteins for basal and Cdc42-regulated FRET efficiency (Fig. 1*b*). The basal FRET signal was eliminated by proteinase K treatment, indicating that this signal is caused by intramolecular interactions (Fig. 1*c*). Removal of 30 residues from the N terminus of N-WASP resulted in maximal Cdc42-induced reduction in FRET efficiency (Fig. 1 *b*, *c*, and *d*). This reporter, which we named Stinger (spatial and temporal imaging of N-WASP-activity via a genetically encoded reporter), was used in all subsequent experiments.

To determine whether the FRET efficiency of Stinger reflected the activation state of N-WASP, we measured the emission profile of Stinger in the presence of Cdc42 and PIP_2, two factors known to bind directly to N-WASP and act cooperatively to increase N-WASP-dependent actin nucleation (10, 12, 14–18). The addition of subsaturating amounts of either Cdc42 or PIP_2 alone to cell extracts containing Stinger resulted in only modest changes in FRET efficiency (Fig. 1*c*). However, the addition of Cdc42 and PIP_2 together resulted in a synergistic decrease in Stinger FRET (Fig. 1c), which reflects the activity changes of N-WASP that have been observed in actin-polymerization assays (10). Further analysis revealed statistically significant differences in FRET efficiency between control versus Cdc42-only-treated extracts, control versus Cdc42- plus PIP_2-treated extracts, and Cdc42-only versus Cdc42- plus PIP_2-treated extracts (Fig. 1*d*, $P < 0.05$, $n = 3$ samples per group, two-sampled *t* test). These results indicate that, similar to the endogenous N-WASP, Stinger can integrate upstream Cdc42 and PIP_2 signals, and integration is reflected in a synergistic change in FRET efficiency.

We then tested whether Stinger could be used to monitor regulated N-WASP activity in live cells. Photobleaching of YFP in HEK-293 cells expressing Stinger resulted in an increase in CFP fluorescence, demonstrating that Stinger exhibited basal FRET in live cells as well as in cell extracts (Fig. 2*a*). HEK-293 cells were transfected with either Stinger alone or Stinger together with Cdc42, and dual-emission ratio fluorescent microscopy was used to measure FRET efficiency. Cells expressing Cdc42 exhibited a statistically significant decrease in Stinger FRET efficiency compared with control cells (Fig. 2*b*, $P < 0.05$, $n = 10$ fields of view, two-sampled *t* test). Furthermore, the Cdc42-induced change in the FRET efficiency in live cells was similar to the Cdc42-induced FRET change observed *in vitro* (Fig. 1*d*). These data demonstrate that N-WASP activity can be determined both in cell extracts and in live cells by monitoring changes in Stinger FRET efficiency.

Because EGF is known to cause cytoskeletal rearrangements in an N-WASP-dependent manner (14, 19, 20), EGF regulation of Stinger FRET was examined in living COS-7 cells expressing Stinger. Dual-emission ratio fluorescence microscopy revealed a maximal increase in whole-cell N-WASP activity 1 min after EGF addition, which then decreased to prestimulation levels by 20 min (Fig. 2 *c* and *d*). Spatially, Stinger FRET revealed activated N-WASP in both the nucleus and the cytoplasm (Fig. 2*c*) of resting and EGF-stimulated cells. Endogenous N-WASP is known to be present in the nucleus (21), and N-WASP was recently found to regulate gene transcription (21), but it is not known whether such regulation is through the direct action of

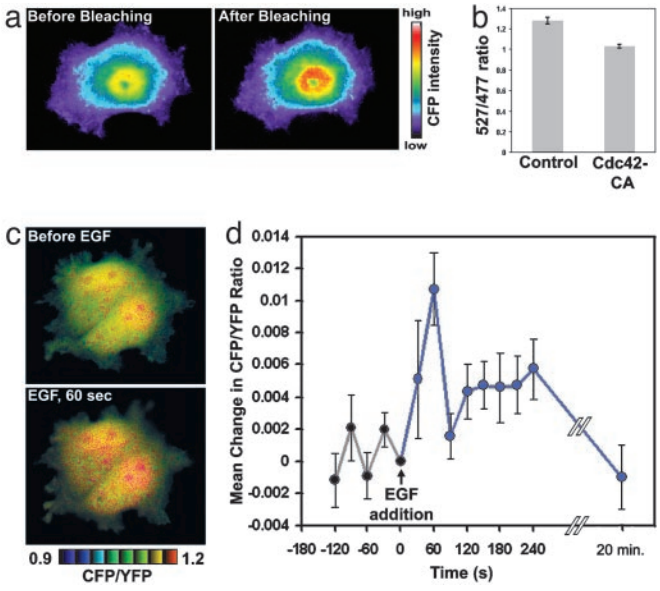

Fig. 2. Stinger can be used to visualize regulated N-WASP activity changes in living cells. (*a*) Stinger undergoes FRET *in vivo*. To verify the existence of intramolecular FRET of Stinger in live HEK-293 cells, CFP emission was visualized before and after YFP photobleaching. CFP emission increased after YFP photobleaching, confirming Stinger FRET. (*b*) Constitutively active Cdc42 causes a reduction of Stinger FRET efficiency in live cells. Live HEK-293 cells expressing either Stinger alone or Stinger plus Cdc42-CA were used for dual-emission ratio imaging. The mean ratio of YFP/CFP emission during CFP excitation was then determined. Ten random fields of view were imaged by using a ×10 objective for each group, each containing 50–100 cells. Error bars represent SEM. (*c*) EGF causes a transient activation of N-WASP in COS-7 cells. Cells expressing Stinger were serum-starved overnight and imaged before and 1 min after addition of 50 ng/ml EGF. FRET efficiency is represented by intensity-modulated display (IMD) coloring, in which CFP/YFP ratio values determine the color of each pixel and intensity values determine the brightness of each pixel. Higher ratio values of CFP/YFP (warm colors) indicate a reduction of FRET efficiency and represent increased N-WASP activity. (*d*) Quantification of N-WASP activation after EGF addition. Cells expressing Stinger were serum-starved overnight and then exposed to 50 ng/ml EGF at time 0. Dual-emission ratio imaging of individual cells was conducted at 1-min intervals before and after stimulation, and the mean CFP/YFP ratio for each cell was then determined. The mean changes in CFP/YFP (compared with time 0) of 19 cells are shown. EGF caused a statistically significant increase in N-WASP activity 1 min after addition (paired *t* test, $P < 0.005$, $n = 19$). Error bars represent SEM.

N-WASP in the nucleus or through indirect effects of N-WASP after regulation of cytoplasmic proteins that could translocate to and act in the nucleus. These results demonstrate that Stinger can be used to visualize spatial and temporal regulation of N-WASP activity by extracellular ligands in live cells.

Having shown that we could reliably monitor N-WASP activity by using Stinger, we then characterized subcellular N-WASP activity in living cells. Membrane ruffles are composed of a complicated network of branched actin filaments thought to be involved in cell migration and macropinocytosis (6, 22), but mechanisms underlying the formation and the regulation of these structures remain largely unknown. We first used fluorescent probes for actin (actin-GFP), PIP_2 (PLC-d1-PH-GFP), and Cdc42 (Raichu 1054x), which showed that constitutively forming ruffles in living COS-7 cells contained high levels of actin, PIP_2, and active Cdc42 (Fig. 3 *a–c* and Movies 1–3). Although it has been shown previously that PIP_2 and actin are enriched in membrane ruffles (23), it had not been demonstrated that Cdc42 is activated in these structures. Through the use of dual-emission ratio time-lapse imaging of Stinger, we discovered that N-WASP

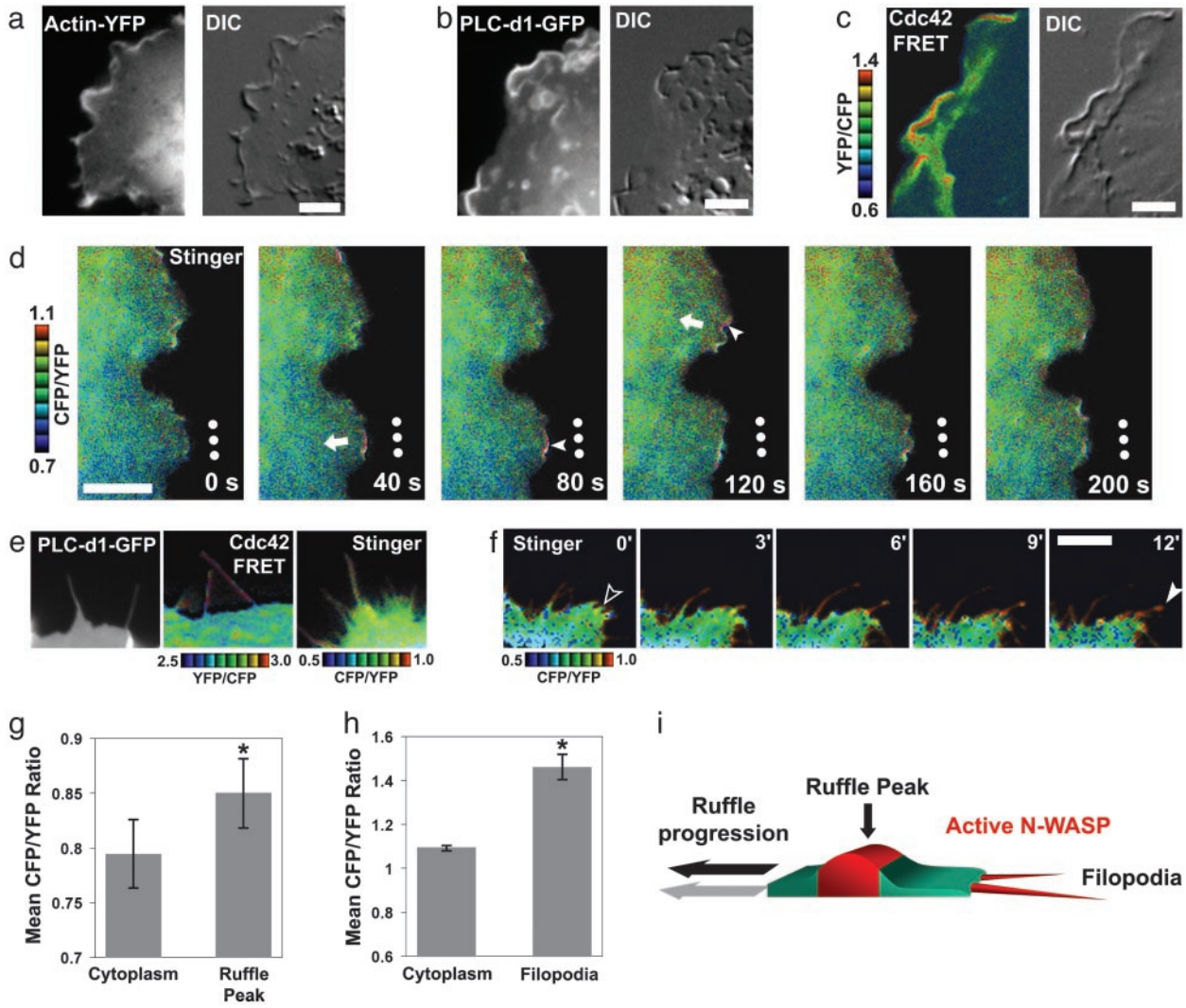

Fig. 3. N-WASP is activated at the peak of inwardly moving membrane ruffles and in protruding filopodia. (*a*) Actin is enriched in membrane ruffles in COS-7 cells. Actin-YFP was expressed in COS-7 cells, and time-lapse microscopy was performed. (Scale bar = 5 μm.) DIC, differential interference contrast. In addition, see Movie 1. (*b*) PIP_2 is enriched in membrane ruffles in COS-7 cells. PLC-d1-GFP, a probe that indicates PIP_2 localization, was expressed in COS-7 cells, and time-lapse microscopy was performed. (Scale bar = 5 μm.) In addition, see Movie 2. (*c*) Cdc42 is activated in membrane ruffles in COS-7 cells. Dual-emission ratio imaging of Raichu-1054x-Cdc42 was performed as described for Fig. 2. Higher ratio values of YFP/CFP (warm colors) indicate activated Cdc42. (Scale bar = 5 μm.) In addition, see Movie 3. (*d*) N-WASP is activated at the peak of inwardly moving membrane ruffles. COS-7 cells expressing Stinger were grown in serum-containing medium and used for dual-emission ratio time-lapse imaging. Higher ratio values of CFP/YFP (warm colors) indicate activated N-WASP. Dots indicate the same stationary points in each frame. Arrows indicate the direction of membrane ruffle translocation. Note the high activity at the areas immediately at the peaks of membrane ruffles (red, filled arrowheads). (Scale bar = 5 μm.) In addition, see Movie 4. (*e*) N-WASP activators are present in filopodia, and N-WASP is active inside of and at the tip of filopodia, compared with the underlying cytoplasm. Serum-starved COS-7 cells were stimulated with 50 ng/ml EGF and imaged 10–30 min after stimulation. PLC-d1-GFP was used to determine PIP_2 localization. Dual-emission ratio imaging of Raichu-1054x was performed as described for *b*. Higher ratio values of YFP/CFP (warm colors) indicate activated Cdc42. Dual-emission ratio imaging of Stinger was performed as described for *d*. Higher ratio values of CFP/YFP (warm colors) indicate activated N-WASP. (*f*) N-WASP is activated inside protruding filopodia. Serum-starved COS-7 cells were stimulated with 50 ng/ml EGF for 10 min and then subjected to dual-emission ratio time-lapse imaging. Higher ratio values of CFP/YFP (warm colors) indicate activated N-WASP. The empty arrowhead indicates an area of new filopodia formation, and the filled arrowhead points to the extending filopodia. (Scale bar = 5 μm.) In addition, see Movie 5. (*g*) Quantification of N-WASP activation in membrane ruffles. Cells were imaged as described for *d*, and the mean CFP/YFP ratios of individual membrane ruffles and the immediately adjacent cytoplasm at single time points were determined. The mean CFP/YFP ratios of 17 separate ruffles in six separate cells were then averaged. *, Statistically significant difference (paired *t* test, $P < 0.005$, $n = 17$). Error bars = SEM. (*h*) Quantification of N-WASP activation in filopodia. Cells were imaged as described for *f*, and the mean CFP/YFP ratios of individual filopodia and the immediately adjacent cytoplasm at single time points were determined. The mean CFP/YFP ratios of 22 separate filopodia in three separate cells were then averaged. *, Statistically significant difference (paired *t* test, $P < 0.005$, $n = 22$). Error bars = SEM. (*i*) Model of N-WASP regulation during membrane ruffle progression and filopodia formation showing a cross section of a membrane ruffle.

was highly active at the peaks of moving ruffles compared with the surrounding cytoplasm (Fig. 3 *d* and *g*). Interestingly, it was recently discovered that WASP-interacting protein (WIP), a protein that is involved in N-WASP-mediated filopodia formation (24), also plays an important role in membrane ruffling (25). Our observations suggest a role for PIP_2, Cdc42, and N-WASP in regulating membrane ruffling, in addition to their proposed roles in microspike/filopodium formation (7).

Although a number of studies have indirectly implicated N-WASP involvement in filopodium formation, and immuno-

cytochemistry has revealed its presence in these structures (7, 26), the role of N-WASP in filopodium formation has not been established (4). Using fluorescent probes for PIP_2 (PLC-d1-PH-GFP) and Cdc42 (Raichu 1054x), we found that EGF-stimulated filopodia in serum-starved COS-7 cells contained PIP_2 and active Cdc42. Through dual emission ratio time-lapse imaging of Stinger, we discovered that N-WASP was active inside of extending filopodia after EGF stimulation of COS-7 cells (Fig. 3 *e*, *f*, and *h*). Because antibody staining has revealed that the Arp2/3 complex is not present in filopodia (27), our results suggest that this particular pool of N-WASP may act through an Arp2/3-independent mechanism.

This study addresses the regulation of N-WASP *in vivo*, and it reveals interesting aspects of N-WASP regulation during cytoskeletal reorganization. It also documents a biosensor that displays activity readouts that are correlated with the integration of multiple upstream signals. Because the regulation of other WASP/WAVE proteins is also achieved by inter- and intramolecular interactions, our work suggests that it should also be possible to monitor their activities through the use of FRET-based reporters. The ability to directly visualize the spatial as well as the temporal regulation of WASP/WAVE activities in living cells at high spatial and temporal resolution provides a powerful tool to investigators studying a number of distinct biological problems such as growth-factor signaling, vesicle trafficking, directed cell migration, axon guidance, and synaptic reorganization.

We are grateful to Drs. Tadaomi Takenawa and Marc Kirschner for their generous gifts of N-WASP constructs, to Michiyuki Matsuda for providing the Cdc42 FRET probe, and to Roger Tsien for providing citrine enhanced YFP. We thank Dr. Greg Longmore, Ernst Ungewickell, Corey McCann, and Brad Miller for helpful comments on the manuscript. This work was supported by grants from the National Institutes of Health (RO1 AG17518), the Society for Progressive Supranuclear Palsy, the National Brain Tumor Foundation, and the Muscular Dystrophy Association (to J.Y.W.) and by a Scholarship from the Leukemia Society of America (to J.Y.W.).

1. Benesch, S., Lommel, S., Steffen, A., Stradal, T. E., Scaplehorn, N., Way, M., Wehland, J. & Rottner, K. (2002) *J. Biol. Chem.* **277,** 37771–37776.
2. Yamaguchi, H., Miki, H. & Takenawa, T. (2002) *Cancer Res.* **62,** 2503–2509.
3. Snapper, S. B., Takeshima, F., Anton, I., Liu, C. H., Thomas, S. M., Nguyen, D., Dudley, D., Fraser, H., Purich, D., Lopez-Ilasaca, M., *et al*. (2001) *Nat. Cell Biol.* **3,** 897–904.
4. Lommel, S., Benesch, S., Rottner, K., Franz, T., Wehland, J. & Kuhn, R. (2001) *EMBO Rep.* **2,** 850–857.
5. Banzai, Y., Miki, H., Yamaguchi, H. & Takenawa, T. (2000) *J. Biol. Chem.* **275,** 11987–11992.
6. Pollard, T. D. & Borisy, G. G. (2003) *Cell* **112,** 453–465.
7. Takenawa, T. & Miki, H. (2001) *J. Cell Sci.* **114,** 1801–1809.
8. Miki, H., Sasaki, T., Takai, Y. & Takenawa, T. (1998) *Nature* **391,** 93–96.
9. Kim, A. S., Kakalis, L. T., Abdul-Manan, N., Liu, G. A. & Rosen, M. K. (2000) *Nature* **404,** 151–158.
10. Prehoda, K. E., Scott, J. A., Mullins, R. D. & Lim, W. A. (2000) *Science* **290,** 801–806.
11. Rohatgi, R., Ho, H. Y. & Kirschner, M. W. (2000) *J. Cell Biol.* **150,** 1299–1310.
12. Rohatgi, R., Ma, L., Miki, H., Lopez, M., Kirchhausen, T., Takenawa, T. & Kirschner, M. W. (1999) *Cell* **97,** 221–231.
13. Moreau, V., Frischknecht, F., Reckmann, I., Vincentelli, R., Rabut, G., Stewart, D. & Way, M. (2000) *Nat. Cell Biol.* **2,** 441–448.
14. Miki, H., Miura, K. & Takenawa, T. (1996) *EMBO J.* **15,** 5326–5335.
15. Symons, M., Derry, J. M., Karlak, B., Jiang, S., Lemahieu, V., McCormick, F., Francke, U. & Abo, A. (1996) *Cell* **84,** 723–734.
16. Ma, L., Rohatgi, R. & Kirschner, M. W. (1998) *Proc. Natl. Acad. Sci. USA* **95,** 15362–15367.
17. Mullins, R. D. & Pollard, T. D. (1999) *Curr. Biol.* **9,** 405–415.
18. Higgs, H. N. & Pollard, T. D. (2000) *J. Cell Biol.* **150,** 1311–1320.
19. Fukuoka, M., Suetsugu, S., Miki, H., Fukami, K., Endo, T. & Takenawa, T. (2001) *J. Cell Biol.* **152,** 471–482.
20. Otsuki, M., Itoh, T. & Takenawa, T. (2003) *J. Biol. Chem.* **278,** 6461–6469.
21. Suetsugu, S. & Takenawa, T. (2003) *J. Biol. Chem.* **278,** 42515–42523.
22. Lee, E. & Knecht, D. A. (2002) *Traffic* **3,** 186–192.
23. Matsuda, M., Paterson, H. F., Rodriguez, R., Fensome, A. C., Ellis, M. V., Swann, K. & Katan, M. (2001) *J. Cell Biol.* **153,** 599–612.
24. Martinez-Quiles, N., Rohatgi, R., Anton, I. M., Medina, M., Saville, S. P., Miki, H., Yamaguchi, H., Takenawa, T., Hartwig, J. H., Geha, R. S. & Ramesh, N. (2001) *Nat. Cell Biol.* **3,** 484–491.
25. Anton, I., Saville, S. P., Byrne, M. J., Curcio, C., Ramesh, N., Hartwig, J. H. & Geha, R. (2003) *J. Cell Sci.* **116,** 2443–2451.
26. Ho, H. Y., Rohatgi, R., Ma, L. & Kirschner, M. W. (2001) *Proc. Natl. Acad. Sci. USA* **98,** 11306–11311.
27. Svitkina, T. M. & Borisy, G. G. (1999) *J. Cell Biol.* **145,** 1009–1026.